PCCP

Accepted Manuscript

ROYAL SOCIETY OF CHEMISTRY

www.rsc.org/pccp

Graphical abstracts:

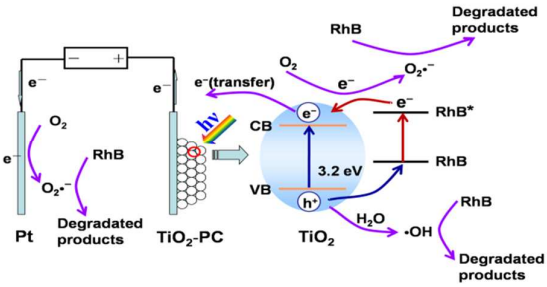

The possible degradation mechanisms of TiO_2 photonic crystal in photoelectrocatalytic and photocatalytic systems were compared and put forward.

Cite this: DOI: 10.1039/c0xx00000x

www.rsc.org/xxxxxx

ARTICLE TYPE

Photoelectrocatalytic degradation of rhodamine B on TiO_2 photonic crystal

Xiuzhen Zheng, Danzhen Li*, Xiaofang Li, Linhui Yu, Peng Wang, Xiaoyun Zhang, Jialin Fang, Yu Shao, and Yi Zheng

Received (in XXX, XXX) Xth XXXXXXXXX 20XX, Accepted Xth XXXXXXXXX 20XX
DOI: 10.1039/b000000x

As the inverse-opal structure facilitates the separation of electron/hole pairs and electron transfer, it may generate many radical species with strong oxidation capability. When a low bias voltage was applied on the TiO_2 electrodes with inverse-opal structure, they exhibited more excellent photoelectrochemical properties and photoelectrocatalytic activity than TiO_2 film under simulated solar light irradiation. When different types of active species scavengers were added, the different performance of TiO_2 photonic crystal for rhodamine B degradation showed that besides •OH and holes, which were the main active species in the photocatalysis, O_2•$^-$ played a vital role in the photoelectrocatalytic degradation process. Furthermore, the stronger signal of •OH-trapping photoluminescence and the variation in the concentration of nitroblue tetrazolium reflected that more •OH and O_2•$^-$ could be generated in the photoelectrocatalysis than that in the photocatalysis, and O_2•$^-$ were partially from the cathode surface. At last, the roles of active species played in the photoelectrocatalytic and photocatalytic process were compared, and the possible degradation mechanisms of TiO_2 photonic crystal in photoelectrocatalytic and photocatalytic systems were put forward, which could provide a good insight into the mechanism of photoelectrocatalytic degradation for TiO_2 photonic crystal.

1 Introduction

Since the discovery of water splitting on titanium dioxide (TiO_2) surfaces by photoirradiation, TiO_2 has attracted extensive interest.[1, 2] In the past few decades, TiO_2 has been extensively studied throughout the world and considered as a promising photocatalyst in the organic pollutant degradation, sewage treatment, and disinfection due to its superior photocatalytic activity. [3-6] To date, various structures of TiO_2, including wires, rods, tubes, flakes, spheres and porous structures, have been fabricated for their special physicochemical properties.[7-13] Among these different shapes, one of the important porous structures is photonic crystal, and TiO_2 photonic crystal (TiO_2-PC) has recently attracted significant interest due to its impressive properties.[14] Since TiO_2-PC possesses unique structural and interesting optical properties, such as large surface area, photonic band gap (PBG) scattering effect, and slow photon effect, it has been widely used in the field of water splitting,[15] solar cells,[16] and pollutants decomposition. [17]

However, the practical application of pure TiO_2-PC is still limited by its large band gap (3.2 eV for anatase) and a fast recombination rate of photogenerated electron/hole (e^-/h^+) pairs. Considerable efforts have been devoted to improving the efficiency of photocatalytic degradation by extending the anatase absorption to visible light,[18] prolonging electron and hole lifetimes through doping and incorporating metals,[19, 20] or increasing surface area by making it mesoporous in the wall.[21] In addition to these chemical modifications, photoelectrocatalysis (PEC) has been proven as a feasible route to solve the difficult problem of the recombination between photogenerated electron/hole pairs, [22-24] which can be used to improve the photocatalytic efficiency of the TiO_2-PC film. When a low bias potential is applied on the TiO_2-PC, it significantly promotes the electron transfer and reduces the recombination of photogenerated electrons and holes. As the photogenerated electrons are driven to the counter electrode via the external circuit, the photogenerated holes are left on the surface of the TiO_2-PC electrode. A large number of active species may be produced, since the interconnected nano-framework and highly ordered channels of TiO_2-PC are well-suited for fully capturing solar energy and supply lots of reaction active sites. However, most of the studies on the TiO_2 film have emphasized on the enhancement of hydroxyl radicals (•OH) or holes and their roles for the PEC degradation of organic pollutants. The effect of superoxide radical anions (O_2•$^-$) has usually been ignored.[25-27] To the best of our knowledge, few works have been reported about the properties of TiO_2-PC in the PEC degradation, and the main active species (O_2•$^-$, •OH, H_2O_2) participating in the PEC system of TiO_2-PC film have not been investigated in detail.

In our work, to compare the PEC and photocatalytic properties for rhodamine B (RhB) degradation, the as-formed TiO_2-PC film was utilized as the working electrode for PEC degradation (Supporting Information, Fig. S1). Several bias voltages between

TiO_2-PC and counter electrode (Pt sheet) were applied to promote photogenerated electrons migrating to the counter electrode through the outer circuit, preventing the recombination of electrons and holes. The position of the conduction band (CB) was approximated from the flat band potential, E_{fb}, measured by the photocurrent onset potential. Meanwhile, PEC activity and stability of TiO_2-PC films and TiO_2 nanoparticle film toward RhB degradation were researched in detail. The possible radical species involved in the PEC and photocatalytic degradation of RhB were investigated by means of adding radical scavengers, photoluminescence (PL) spectra, electron spin resonance spectra (ESR) techniques, N,N-diethyl-p-phenylenediamine (DPD) method and nitroblue tetrazolium (NBT) tests. Furthermore, the effect of active oxygen radicals participating in the PEC and photocatalysis system was compared and discussed, and the possible mechanism was proposed.

2. Experimental sections

2.1 Materials

All solvents and chemicals were of analytical grade. Titanium isopropoxide and diethanolamine (Aldrich, 98%) were used as the precursors to prepare TiO_2 colloid. Potassium acetate (AcOK), tert-Butyl alcohol (TBA), ethylenediaminetetraacetic acid (EDTA), and benzoquinone (BQ) were from Sinopharm Chemical Reagent Co., Ltd. 5,5-dimethyl-1-pyrroline-N-oxide (DMPO), horseradish peroxidase (POD) and N,N-diethyl-p-phenylenediamine (DPD) were from J&K Chemical Ltd. Water used in all experiments was deionized water.

2.2 Preparation of TiO_2-PCs

Monodisperse polystyrene (PS) latex spheres with diameters of 270, 340, and 400 nm (denoted as PS270, PS340, and PS400) were synthesized from styrene by a modified emulsifier-free emulsion copolymerization method. The PS opal templates were fabricated by the method of vertical deposition (Fig. S2).[17] The fluorine–tin–oxide (FTO, 20 × 50 × 2 mm^3) conductive glasses were treated in Piranha solution (H_2SO_4/H_2O_2, 7:3) for 24 h, following cleaned with ethanol and deionized water to make its surface hydrophilic, and dried with nitrogen to keep its surface pure. The clean substrate was submerged vertically into the monodisperse PS latex solution (ca. 0.05 wt %) at 45 °C in an oven for the growth of the PS opal template film.

The TiO_2-PCs were synthesized via a facile sandwich method, and the TiO_2 colloidal solution was composed of titanium isopropoxide, ethanol and diethanolamine, the mass ratio of which was 1:2.5:0.12. The FTO glass with PS colloidal crystal on its surface was covered by another microslide, and a small spacer was used to separate them. Then, the FTO with the microslide was put into a beaker containing a small amount of TiO_2 colloid. In this case, the TiO_2 precursor fully occupied the remaining space inside the PS spheres, and then hydrolyzed slowly by air humidity. After filled several times, the TiO_2/PS opal composites were prepared. Subsequently, the sample was calcined at 500 °C for 2 h at a heating rate of 1 °C/min, and TiO_2-PCs were obtained. For the sake of simplicity, TiO_2-PCs with different pore sizes were denoted as T270, T340 and T400 (corresponding for the TiO_2-PCs fabricated using PS270, PS340, and PS400 templates), respectively.

The TiO_2 film was prepared by the same method with the TiO_2-PCs. The difference was that the TiO_2 colloidal solution was composed of titanium isopropoxide, ethanol, diethanolamine, and water, the mass ratio of which was 1:2.5:0.12:0.01. As shown in Fig. S3, the TiO_2 film was composed of TiO_2 nanoparticles.

2.3 Characterization of samples

The general morphologies of the products were examined by field emission scanning electron microscopy (FESEM) on a SU 8000 instrument operated at 5 kV. The X-ray diffraction (XRD) patterns were recorded on a Bruker D8 Advance X-ray diffractometer using Cu $K_{\alpha 1}$ irradiation (λ=1.5406 Å), to identify the phase constitutions in samples. The photoluminescence (PL) spectra were collected on an Edinburgh FL/FS900 fluorescence spectrometer. The generation of •OH was investigated by the PL technique with terephthalic acid (TA) as a probe molecule. The optimal concentration of TA solution was 5×10^{-3} M in a diluted NaOH aqueous solution (1×10^{-2} M).[28, 29] Electron spin resonance (ESR) spectra were obtained using a Bruker model A300 spectrometer with a 500 W Xe-arc lamp equipped with an IR-cutoff filter (320 nm < λ < 800 nm) as light source. Nitroblue tetrazolium (NBT, 2×10^{-5} M, exhibiting an absorption maximum at 259 nm) was used to determine the amount of $O_2^{\bullet-}$ generated from PEC and photocatalytic system.[30, 31] The method was similar to the latter photocatalytic activity test with NBT replacing the RhB. H_2O_2 was determined by a photometric method in which DPD is oxidized by a POD catalyzed reaction, with the absorption peaks at 510 and 551 nm.[32] After 30 min of simulated solar light irradiation, the TiO_2 film was removed from the TiO_2/H_2O system, and the water was analyzed to detect the formation of H_2O_2. The intermediates were detected by LC-MS (LCQ Fleet; Thermo Fisher Scientific Inc., Waltham, MA) equipped with an electrospray ionization positive ion mode. The samples were chromatographically separated using a C18 column (5 μm × 250 mm × 2.0 mm, Thermo Fisher Scientific Inc.) at a flow rate of 200 μL/min. The mobile phase was composed of acetic acid solution (0.1%, V/V) and methanol, and the volume percent of methanol was increased from 35% to 80% within 15 min. The final products were also detected by a gas chromatograph interfaced with a mass spectrometer (GC/MS 5973, Hewlett-Packard Inc., USA). The MS was operated with an electron impact (EI) in positive ion mode. The pre-treatment process was as follows: the reacted solution was adjusted pH to 2.0 with 10% HCl solution, extracted with dichloromethane for three times, and dehydrated by using anhydrous sodium sulphate.

2.4 Tests of PEC activity

Photoelectrochemical measurements were carried out on a CHI 660D electrochemical system (Chenhua Instruments, Co., Shanghai). The testing system was comprised of three electrodes and a single-compartment quartz cell (2.8 × 2.8 × 4.3 cm^3), using 0.05 mol/L Na_2SO_4 as the electrolyte. A thin film of TiO_2-PC or TiO_2 nanoparticle with the same area of 2 × 3 cm^2 was employed as the working electrode. A platinum sheet (2 × 4.5 cm^2) was used as a counter electrode with saturated calomel electrode (SCE) as the reference electrode.

In the test of PEC activity, the light source was a 500 W Xe-arc lamp (Institute of Electric Light Source, Beijing) and an 800 nm cutoff filter was placed in front of the quartz cell to ensure that

irradiation of organic pollutant/TiO_2 system occurred under simulated solar light irradiation (320 nm < λ < 800 nm, Fig. S4). The initial concentration of the RhB solution was 5 ppm (20 mL), and dark (adsorption) experiments were carried out for 30 min to reach adsorption–desorption equilibrium. A small aliquot was withdrawn at each given time interval and analyzed using a Varian Cary 50 Scan UV-Vis spectrophotometer. After the concentration of the solution was monitored by the absorption peak at 554 nm, the analyzed aliquot was quickly poured back into the reactor. The PEC and photocatalytic degradation ratio is recognized as $(1-C_t/C_0)\times100\%$, where C_0 is the adsorption equilibrium concentration of solution, and C_t is the concentration of solution at time t.

3 Results and discussion

3.1 Morphologies and Transmittance Spectra of TiO_2-PCs

SEM images of the as-prepared TiO_2-PCs were shown in Fig. 1. From the SEM images, it could be observed that TiO_2-PCs well duplicated the highly ordered structure of PS templates to form an ordered skeleton structure. The average pore sizes of TiO_2-PCs were about 200, 220, and 270 nm, corresponding to the T270, T340, and T400 samples, respectively. The PBGs for TiO_2-PCs arising from the highly-ordered periodic structure were measured by transmittance spectra (Fig. 1d). The PBG peaks of TiO_2-PCs (T270, T340, and T400) were centered at around 450, 557, and 630 nm, respectively. Herein, the PBG of T340 was precisely designed to overlap with the absorption peaks of RhB (554nm). Moreover, TiO_2-PCs and TiO_2 nanoparticles had similar XRD patterns, and the characteristic diffraction peaks were assigned to the crystallographic planes of anatase TiO_2 (Fig. S5, CPDS card No. 21-1272).

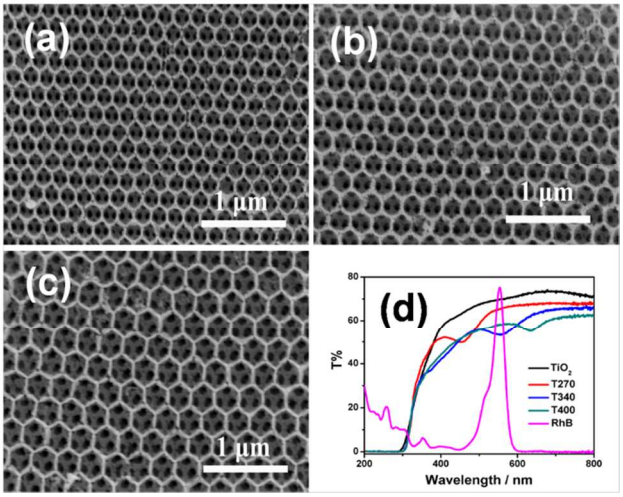

Fig. 1 SEM images of the TiO_2-PCs with different pore sizes: (a) T270, (b) T340, (c) T400, and the transmittance spectra (d) of TiO_2 samples measured in water.

3.2 Photoelectrochemical Measurement

The position of the semiconductor band is an important physical property for semiconductor. Herein, the flat band potential (E_{fb}) was measured using the photocurrent onset potential for TiO_2 films.[33] Typically, when the surface of the semiconductor electrode and solution interface are contacted, the surface band bends to form a built-in electric field. According to the mechanism of photocurrent, photo-generated electrons migrate to form the photocurrent in the effect of built-in electric field. When a reverse bias is applied, it can offset part of the built-in electric field. As the built-in voltage approaches zero, the current is zero, and the external voltage at this time is equal to the flat band. Therefore, ignoring the deviation of flat band and conduction band potential (E_{cb}), it can be considered that the position of the conduction band is approximated the position of the flat band potential.

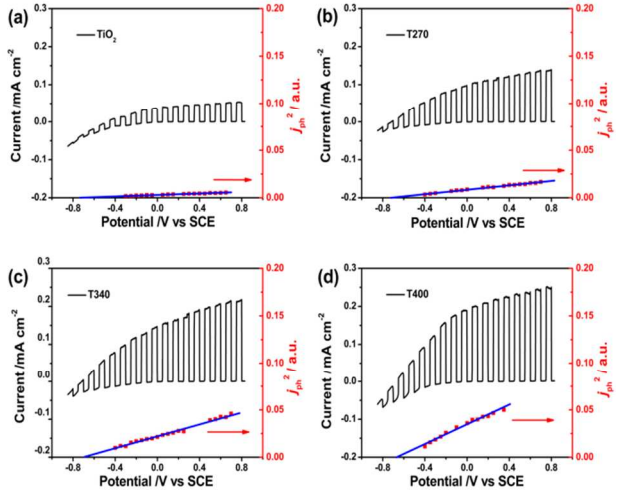

Fig. 2 E_{fb} measurements of TiO_2 (a) and TiO_2-PCs (b-d) by the photocurrent (j_{ph}) onset method using the fit to Buttler theory for j_{ph}^2 in mixture electrolyte of 1 mol•L^{-1} Na_2SO_4 and 1 mol•L^{-1} AcOK under simulated solar light illuminaion (scan rate of 2 mV/s, scan from positive side, and light intensity of 0.30 W/cm^2).

E_{fb} was measured using the photocurrent onset potential for TiO_2 films in aqueous solution. Fig. 2 showed the photocurrent of TiO_2 films in mixture electrolyte of 1 mol•L^{-1} Na_2SO_4 and 1 mol•L^{-1} AcOK with the simulated solar light intensity of 0.30 W/cm^2. By alternating light and dark measures of linear sweep photovoltammetry (LSV), a step change could be measured by photocurrent density (j_{ph}) with the scan. From the onset of j_{ph}, the Buttler method was used to calculate E_{fb} with equation ($j_{ph}^2 \sim (E - E_{fb})$), and j_{ph}^2 was proportional to the potential E. [33, 34] The square of the j_{ph} vs E would have an x intercept of E_{fb}. As shown in Fig. 2, E_{fb} of TiO_2, T270, T340, and T400, were -0.73 V, -0.70 V, -0.67 V, and -0.65 V vs. SCE, respectively. To further calculate, they are -0.49 V, -0.46 V, -0.43 V, and -0.41 V vs. NHE. Thereby, E_{cb} of TiO_2, T270, T340, and T400 were about -0.49 V, -0.46 V, -0.43V, and -0.41 V, respectively. As the band gap for anatase TiO_2 is recognized as 3.2 eV, according to the formula $E_g = E_{vb} - E_{cb}$, the corresponding valence band potentials (E_{vb}) for TiO_2 films were 2.71 V, 2.74 V, 2.77 V, and 2.79 V, which was shown in Table 1. The E_{vb} of TiO_2 samples followed the order T400 > T340 > T270 > TiO_2, which were more positive than the standard redox potential of •OH/OH^- (2.38 V vs NHE). As the top of the valence band is more positive, the oxidative capacity of holes is stronger. The sources of •OH radical were investigated, which were mainly from two ways. One was the reaction between holes and surface hydroxyl groups ($h_{vb}^+ + H_2O$ (OH^-) → •OH + H^+, Fig. S6), and the other one was the

decomposition of adsorbed H_2O_2 ($e^- + H_2O_2 + H^+ \rightarrow$ •OH + H_2O, Fig. S7). The sources of •OH radical revealed similar trend to the order of their E_{vb}, illuminating that the TiO_2-PCs possessed the higher separation efficiency of electron/hole pairs and more amount of active species than TiO_2 nanoparticles.

Table 1 the flat band, conduction and valence band potentials of TiO_2-PCs and TiO_2 nanoparticle film:

sample	TiO_2	T270	T340	T400
E_{fb} vs. SCE	-0.73 V	-0.70V	-0.67V	-0.65V
E_{fb} vs. NHE	-0.49 V	-0.46 V	-0.43 V	-0.41 V
E_{cb} vs. NHE	-0.49V	-0.46 V	-0.43 V	-0.41 V
E_{vb}vs. NHE	2.71V	2.74V	2.77 V	2.79 V

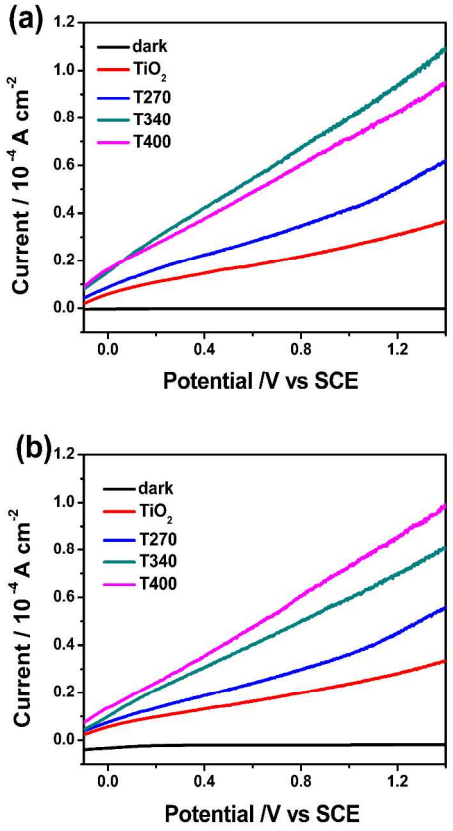

Fig. 3 Photocurrent generation versus bias potential (vs SCE) obtained from TiO_2-PCs and TiO_2 electrodes in 0.05 mol/L Na_2SO_4 with RhB solution (a) and without RhB solution (b) under simulated solar light illumination (the scan rate of 0.02 V/s, and light intensity of 0.30 W/cm^2).

Photocurrent densities as a function of applied potential of TiO_2-PCs and TiO_2 electrodes were investigated by LSV, which demonstrated the electron generation capacity and electron transfer effectiveness. As shown in Fig. 3a (RhB and Na_2SO_4 solution) and Fig. 3b (Na_2SO_4 solution), the dark current density was found to be negligible. With the increase of applied voltage, the photocurrent of TiO_2 electrodes in the dye and Na_2SO_4 solution increased more rapidly than that in Na_2SO_4 solution. The significantly improvement of photocurrent could be attributed to the effect of dye sensitization. Specially, the T340 electrode increased most rapidly among all of the TiO_2 electrodes. As previous work reported, when the PBG of T340 was matched with the absorption peak of RhB, dye sensitization could be intensified by slow photon effect on the edges of PBG.[17] As a result, T340 performed better photoelectric synergistic effect than other TiO_2 electrode, and the reason was that the dye sensitization of RhB was significantly enhanced by slow photon effect when bias voltage was applied.

3.3 PEC Activity and Stability of TiO_2-PCs

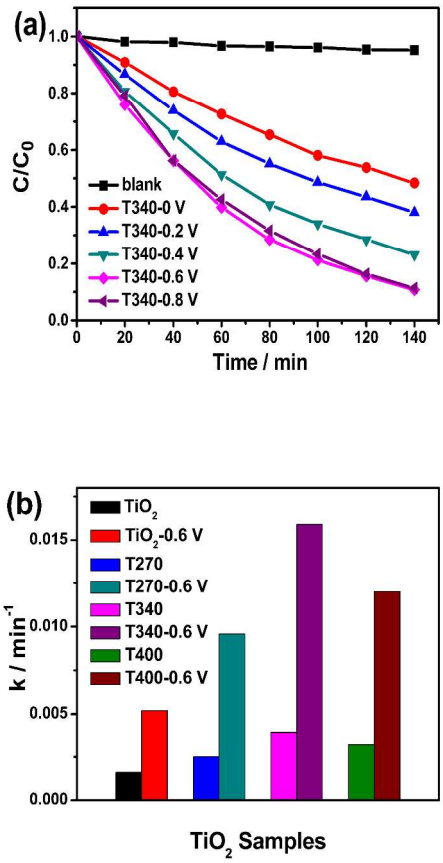

Fig. 4 (a) PEC degradation of T340 with different applied bias voltages and (b) kinetic constants (k) of TiO_2 samples for PEC and photocatalytic degradation under simulated solar light irradiation.

In the PEC process, the applied voltage could efficiently transfer the photogenerated electrons to the counter electrode, preventing the recombination of electrons and holes. Then, the applied voltage was an important factor for PEC degradation. As shown in Fig. 4a, five different voltages, 0, 0.2, 0.4, 0.6, and 0.8 V, were investigated on T340 for RhB degradation. The results showed that when the applied voltage was increased from 0 to 0.6 V, the degradation ratios of RhB increased rapidly from 51.6% to 89.2%. However, when the applied voltage further increased to 0.8 V, the degradation ratio was slightly reduced. It indicated that the photoinduced carrier reached sufficient separation when the voltage was applied to 0.6 V. Once the photocurrent exceeded 0.6 V, the degradation efficiency would not increase with the increase of bias voltage but decrease. Therefore, under the bias voltage of 0.6 V, T340 electrode exhibited excellent photocatalytic activity toward the RhB degradation under simulated solar light irradiation.

Cite this: DOI: 10.1039/c0xx00000x

www.rsc.org/xxxxxx

ARTICLE TYPE

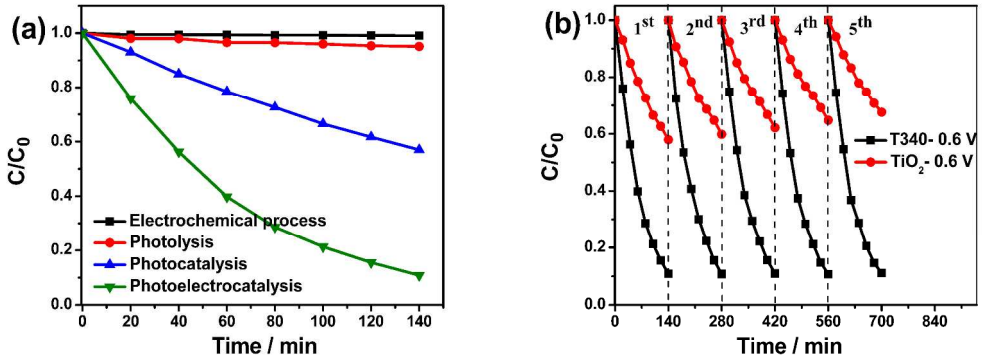

Fig. 5 (a) Electrochemical process, photolysis, photocatalysis and PEC degradation of T340 film, and (b) PEC stable activity over T340-0.6 V and TiO_2-0.6 V under simulated solar light irradiation.

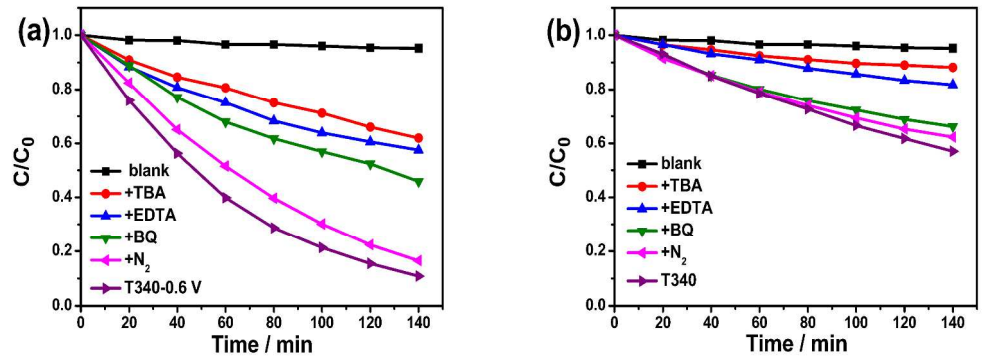

Fig. 6 PEC (a) and photocatalytic (b) degradation of RhB for T340 under different conditions under simulated solar light irradiation.

To further evaluate the PEC capability of TiO_2-PCs, TiO_2 nanoparticle film was used as the reference catalyst. As displayed in Fig. 4b, under the bias voltage of 0.6 V, the PEC and photocatalytic degradation processes of TiO_2-PCs film and TiO_2 film were fit for pseudo-first-order kinetics by linear transforms formula $-\ln (C_t/C_0) = kt$, and the apparent rate constant k were shown in table S1. The TiO_2-PCs showed higher PEC activity for RhB degradation than TiO_2 nanoparticles as a synergistic result of the large specific surface areas, the enhanced mass transfer and electron transfer. Furthermore, the visible-light activity of photocatalysis and PEC was clearly observed from the RhB degradation (Fig. S8), and this was the result of dye sensitization. T340 possessed the best photocatalytic activity whether in the simulated solar light or visible light irradiation among all of the TiO_2-PCs. This could be attributed to the dye absorption intensified by slow photon effect on PBG edges of T340 (Fig. S9). Meanwhile, T340 possessed the best PEC activity, as slow photon effect was participated in the degradation process when bias voltage was applied. It reconfirmed the LSV result that dye sensitization of RhB significantly enhanced by the slow photon effect in the presence of electric field.

The electrochemical process, photolysis (without photocatalyst), photocatalysis and PEC degradation in the RhB solutions were performed on the T340 under simulated solar light illumination (Fig. 5a). In the PEC process, when the bias voltage of 0.6 V was applied, 89.2 % of RhB was degraded after 140 min (Fig. S10). While only 43.0 % and 1.3 % of RhB were removed in photocatalytic and electrochemical process during the same time. Thus, the RhB degradation rate in the PEC process was much faster than the summation of photocatalysis and electrochemical process. Such synergetic effect between photocatalytic and EC proved PEC as a feasible route to improve the RhB degradation efficiency. In addition, the degradation intermediates of RhB in PEC and photocatalytic processes were identified by LC/MS and GC/MS (Fig. S11-S14). It was found that the final products detected in the PEC process were less than those in the photocatalytic degradation on T340, indicating that PEC exhibited higher degradation efficiency. Besides, T340-0.6 V also

Cite this: DOI: 10.1039/c0xx00000x

www.rsc.org/xxxxxx

ARTICLE TYPE

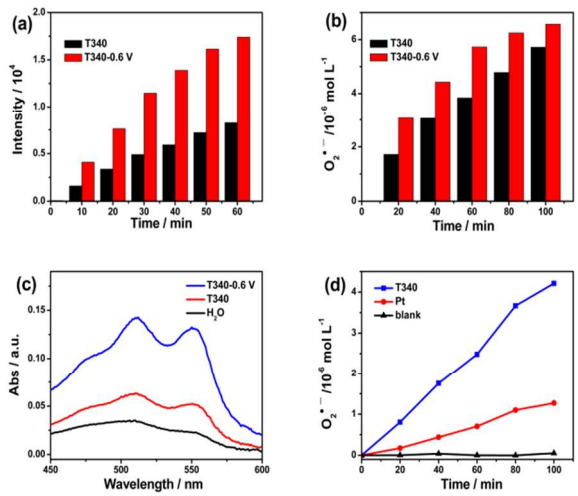

Fig. 7 (a) •OH-trapping PL intensity of T340-0.6 V and T340 in TA solution. (b) Change of O_2•$^-$ concentration for T340 and T340-0.6 V. (c) Absorption spectra of the DPD/POD reagent after reaction with T340 and T340-0.6 V after 0.5 h irradiation. (d) The concentration of O_2•$^-$ for T340 film (under light irradiation) and Pt electrode (without light irradiation) that were separated and connected through the salt bridge.

exhibited better PEC stability than TiO_2 film in the cycling runs of RhB degradation reaction (Fig. 5b). These results indicated that T340 as photonic crystal electrode possessed not only high photocatalytic activity, but also good stability.

3.4 Discussion of PEC and Photocatalytic Mechanism

The presence of inverse-opal structure in the T340 facilitates the separation of electron/hole pairs and electron transfer, which may generate more radical species with strong oxidation capability. ESR spin-trapping technique with DMPO was carried out to detect the active species, and demonstrated •OH and O_2•$^-$ participated in the degradation process (Fig. S15). In order to further confirm that, the role of the active species, such as electrons/holes, •OH and O_2•$^-$, were investigated in PEC and photocatalytic degradation process. Fig. 6 exhibited the PEC and photocatalytic activity of T340 toward the RhB degradation after different radical scavengers being added. In the PEC degradation (Fig. 6a), the RhB degradation rate was 89.2% without the addition of the scavengers. Tert-butyl alcohol (TBA) is considered as an excellent capturer of •OH, and can be easily oxidized by •OH.[35] The addition of TBA (500 μL) led to the most inhibition of the RhB degradation, illuminating that •OH played the most important role in the PEC degradation process. Holes are another reactive species in photocatalytic reactions, which can be captured by ethylenediaminetetraacetic acid (EDTA).[25] After adding EDTA into the system (1×10^{-3} mol/L), the PEC degradation process was remarkably inhibited. The benzoquinone (BQ) had the ability to trap O_2•$^-$ by a simple electron transfer mechanism.[31, 36] The addition of BQ (0.2 mg) partially inhibited RhB degradation, indicating that O_2•$^-$ was significant in the PEC process. Moreover, dissolved O_2 is an electron-capturer to produce a variety of active oxygen species, and promotes the degradation process. In order to evaluate the role of dissolved O_2 in the reaction, N_2 was bubbled through the suspension at the rate of 5 mL/min to ensure that the reaction was operated without O_2. Based on the above analysis, it could be concluded that the degradation of RhB was driven mainly by •OH, holes and O_2•$^-$.

However, in photocatalytic degradation (Fig. 6b), after the same amount of TBA and EDTA being added in the system, it obviously affected the degradation rate. However, when BQ was added, it inhibited the RhB degradation rate to a lesser degree. Thereby, the RhB degradation was driven mainly by the participation of holes and •OH radicals, and O_2•$^-$ radicals to a lesser extent.

As mentioned above, •OH radicals played the most important role in the PEC and photocatalytic degradation process. PL-TA technique was used to monitor the amount of •OH in the PEC and photocatalytic systems, which has been widely used in the detection of •OH.[37] Fig. 7a showed the PL intensity of T340-0.6 V and T340 in aqueous TA solution. It was found that the intensity of T340-0.6 V was about twice of that of T340, indicating that PEC process produced more amount of •OH.

To further ascertain the change of O_2•$^-$, a colorless molecular probe, nitroblue tetrazolium (NBT) was chosen to quantify the O_2•$^-$ concentration produced by T340-0.6 V and T340 under simulated solar light irradiation.[30, 31] Fig. S16 showed the variation of NBT concentration, and the decrease of NBT concentration indicated the generation of O_2•$^-$. It was found that the production rate of O_2•$^-$ for T340-0.6 V was much higher than that of T340 (Fig. 7b). Additionally, the amount of H_2O_2 for T340-0.6 V was much more than that of T340 (Fig. 7c), in accord with the result of the O_2•$^-$ production. Furthermore, when T340 film (light irradiation) and Pt electrode (without light irradiation) was separated and connected through a salt bridge, O_2•$^-$ were produced in T340 film and Pt electrode (Fig. 7d and Fig. S17). By analyzing the amount of active radicals, it could be found that PEC process was beneficial for the separation of photogenerated electron/hole pairs and the production of •OH and O_2•$^-$, which might be the main reason that T340 exhibited excellent PEC activity toward the RhB degradation.

Based on the results of the addition of active species scavengers, ESR, PL-TA, DPD method and NBT test, the mechanisms of PEC and photocatalytic degradation for RhB on TiO_2-PC were proposed. In the photocatalytic system, when TiO_2-PC was excited, a large number of electrons and holes were produced in the system. The photogenerated holes on TiO_2-PC could directly oxidize water to generate •OH radicals and excited electrons reacted with the O_2 adsorbed on the surface of TiO_2-PC to generate O_2•$^-$. Besides, the recombination rate of electrons/hole pairs was high, which hindered its photocatalytic efficiency in RhB degradation.

However, in PEC system, the photogenerated electrons in the

excited TiO_2-PC film were taken away to the Pt electrode under the effect of electric field. Meanwhile, the photogenerated holes were left at the surface of the TiO_2-PC electrode to improve the efficiency of oxidation (i.e., reaction with holes to generate •OH), which was the main source of •OH. Additionally, the sources of O_2•$^-$ were twofold at least: (1) the injected electron reacted with the O_2 adsorbed on the surface of Pt electrode, and (2) the departed photoinduced electrons reacted with the O_2 adsorbed on the surface of TiO_2-PC electrode. In this case, PEC process could solve the problem of the recombination of photogenerated electron/hole pairs in the photocatalysis (equation 4), and the inverse-opal structure was beneficial for the production of active species, such as •OH and O_2•$^-$ (equation 7, 8 and 10).

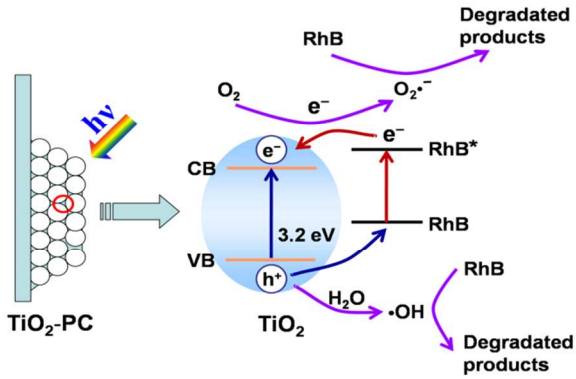

Scheme 1. Possible mechanism of the photocatalytic degradation on TiO_2-PC film under simulated solar light irradiation.

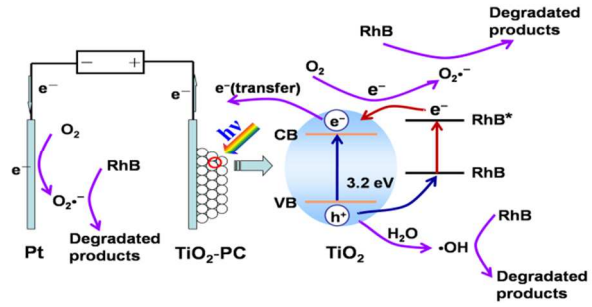

Scheme 2. Possible mechanism for the PEC degradation on TiO_2-PC film under simulated solar light irradiation.

As dye sensitization was important in the RhB degradation whether in the PEC or photocatalytic system, the mechanism and the formulae on TiO_2-PC film of PEC (photocatalytic) reaction were involved and present it. In the TiO_2-RhB system, the lowest unoccupied molecular orbital of RhB could couple with CB of the TiO_2 semiconductor. In this case, electrons could be transferred easily from the excited dyes to the CB of TiO_2 and subsequently generate reactive oxidation species. From all these analyses, the possible degradation mechanisms of TiO_2-PC in the photocatalytic and PEC systems were put forward (Scheme 1 and Scheme 2). The formulae of photocatalytic and PEC reactions were as following:

In photocatalytic system,

TiO_2-PC + hν ⟶ TiO_2-PC ($h^+ + e^-$) (1)

$h^+ + OH^-$ ⟶ •OH (2)

$e^- + O_2$ ⟶ O_2•$^-$ (3)

RhB + hν ⟶ RhB* (4)

$h^+ + e^-$ ⟶ radiative or non-radiative recombination (5)

•OH, h^+ or O_2•$^-$ + Dye ⟶ degraded products (6)

In PEC system,

The anode reaction:

TiO_2-PC + hν (> Eg) ⟶ TiO_2 ($h^+ + e^-$) (7)

$h^+ + H_2O$ ⟶ •OH+ H^+ (8)

$e^- + O_2$ ⟶ O_2•$^-$ (9)

RhB + hν ⟶ RhB* (10)

TiO_2-PC (e^-) + external electrostatic field ⟶ external circuit (11)

The cathode reaction:

$e^- + O_2$ ⟶ O_2•$^-$ (12)

•OH, h^+, or O_2•$^-$ + Dye ⟶ degraded products (13)

4 Conclusions

In summary, PEC, as a feasible route to solve the difficult problem of the recombination between photogenerated electron/hole pairs, is an efficient method to improve the photocatalytic efficiency of the TiO_2-PC film. The TiO_2-PC electrode exhibited more excellent PEC activity and stability than TiO_2 film toward the RhB degradation under simulated solar light irradiation by applying a bias voltage of 0.6 V. In addition, TiO_2-PC showed different properties in the PEC and photocatalytic degradation of RhB. Through investigating the additional conditions (TBA, EDTA, BQ, and N_2) in the degradation process, different results were presented in these two systems because of the effect of active species. It was found that besides •OH and holes, which were the main active species in the PEC and photocatalytic systems, O_2•$^-$ played a vital role in the photoelectrocatalytic degradation process. From PL-TA technique, DPD method and NBT tests, more •OH, H_2O_2 and O_2•$^-$ were generated in the photoelectrocatalysis than that in the photocatalysis. The differences between these two systems lead us to deeply realize the active species and the degradation mechanism in photocatalytic process. At last, the different degradation mechanisms of TiO_2-PC in PEC and photocatalytic systems were put forward. We believe that TiO_2 photonic crystal is expected to be a good prospect in the applications of solar cells, water splitting, as well as PEC degradation.

Acknowledgements

This work was financially supported by the National Natural Science Foundation of China (No: 21173047 and 21373049), and the National Basic Research Program of China (No: 2013CB632405).

Notes and references

Research Institute of Photocatalysis, State Key Laboratory of Photocatalysis on Energy and Environment, Fuzhou University, Fuzhou, 350002, P. R. China, Fax & Tel: (+86)591-83779256; E-mail: dzli@fzu.edu.cn

† Electronic Supplementary Information (ESI) available: [The properties of probe molecules and additional datas]. See DOI: 10.1039/b000000x/

1. A. Fujishima and K. Honda, *Nature*, 1972, **238**, 37-38.
2. M. R. Hoffmann, S. T. Martin, W. Choi and D. W. Bahnemann, *Chem. Rev.*, 1995, **95**, 69-96.
3. M. Tamimi, S. Qourzal, A. Assabbane, J. M. Chovelon, C. Ferronato and Y. Ait-Ichou, *Photoch. Photobio. Sci.*, 2006, **5**, 477-482.

4. Y.-M. Lin, Y.-H. Tseng, J.-H. Huang, C. C. Chao, C.-C. Chen and I. Wang, *Environ. Sci. Technol.*, 2006, **40**, 1616-1621.
5. D. F. Ollis, E. Pelizzetti and N. Serpone, *Environ. Sci. Technol.*, 1991, **25**, 1522-1529.
6. K. Sunada, Y. Kikuchi, K. Hashimoto and A. Fujishima, *Environ. Sci. Technol.*, 1998, **32**, 726-728.
7. J. Z. Chen, W. Y. Ko, Y. C. Yen, P. H. Chen and K. J. Lin, *ACS nano*, 2012, **6**, 6633-6639.
8. S. A. Berhe, S. Nag, Z. Molinets and W. J. Youngblood, *ACS Appl. Mater. Inter.*, 2013, **5**, 1181-1185.
9. N. Lu, X. Quan, J. Li, S. Chen, H. Yu and G. Chen, *J. Phys. Chem. C*, 2007, **111**, 11836-11842.
10. T. Sasaki, S. Nakano, S. Yamauchi and M. Watanabe, *Chem. Mater.*, 1997, **9**, 602-608.
11. X. Jiang, T. Herricks and Y. Xia, *Adv. Mater.*, 2003, **15**, 1205-1209.
12. H. Choi, M. G. Antoniou, M. Pelaez, A. A. de la Cruz, J. A. Shoemaker and D. D. Dionysiou, *Environ. Sci. Technol.*, 2007, **41**, 7530-7535.
13. X. Chen and S. S. Mao, *Chem. Rev.*, 2007, **107**, 2891-2959.
14. F. Sordello, V. Maurino and C. Minero, *Molecular Photochemistry - Various Aspects,* InTech Europe, 2012.
15. J. Liu, G. Liu, M. Li, W. Shen, Z. Liu, J. Wang, J. Zhao, L. Jiang and Y. Song, *Energ. Environ. Sci.*, 2010, **3**, 1503.
16. E. S. Kwak, W. Lee, N.-G. Park, J. Kim and H. Lee, *Adv. Funct. Mater.*, 2009, **19**, 1093-1099.
17. X. Zheng, S. Meng, J. Chen, J. Wang, J. Xian, Y. Shao, X. Fu and D. Li, *J. Phys. Chem. C*, 2013, **117**, 21263-21273.
18. G. Liao, S. Chen, X. Quan, H. Chen and Y. Zhang, *Environ. Sci. Technol.*, 2010, **44**, 3481-3485.
19. J. Xu, B. Yang, M. Wu, Z. Fu, Y. Lv and Y. Zhao, *J. Phys. Chem. C*, 2010, **114**, 15251-15259.
20. Y. Lu, H. Yu, S. Chen, X. Quan and H. Zhao, *Environ. Sci. Technol.*, 2012, **46**, 1724-1730.
21. J. Liu, M. Li, J. Wang, Y. Song, L. Jiang, T. Murakami and A. Fujishima, *Environ. Sci. Technol.*, 2009, **43**, 9425-9431.
22. Z. Zhang, Yuan, G. Shi, Y. Fang, L. Liang, H. Ding and L. Jin, *Environ. Sci. Technol.*, 2007, **41**, 6259-6263.
23. X. Quan, S. Yang, X. Ruan and H. Zhao, *Environ. Sci. Technol.*, 2005, **39**, 3770-3775.
24. S. K. Mohapatra, K. S. Raja, V. K. Mahajan and M. Misra, The *J. Phys. Chem. C*, 2008, **112**, 11007-11012.
25. Y. Hou, X. Li, Q. Zhao, G. Chen and C. L. Raston, *Environ. Sci. Technol.*, 2012, **46**, 4042-4050.
26. Y. Xin, H. Liu, L. Han and Y. Zhou, *J. Hazard. Mater.*, 2011, **192**, 1812-1818.
27. L. Gomathi Devi, N. Kottam, S. Girish Kumar and K. S. Anantha Raju, *Catal. Lett.*, 2009, **131**, 612-617.
28. W. Li, D. Li, Y. Lin, P. Wang, W. Chen, X. Fu and Y. Shao, *J. Phys. Chem. C*, 2012, **116**, 3552-3560.
29. T. Hirakawa and Y. Nosaka, *Langmuir*, 2002, **18**, 3247-3254.
30. H. S. Choi, J. W. Kim, Y. N. Cha and C. Kim, *J.immunoass. immunoch.*, 2006, **27**, 31-44.
31. E. Gao and W. Wang, *Nanoscale*, 2013, **5**, 11248-11256.
32. H. Bader, V. Sturzenegger and J. Hoigné, *Water Res.*, 1988, **22**, 1109-1115.
33. M. A. Alpuche-Aviles and Y. Wu, *J. Am. Chem. Soc.*, 2009, **131**, 3216-3224.
34. M. A. Butler, *J. Appl. Phys.* 1977, **48**, 1914
35. W. Li, D. Li, W. Zhang, Y. Hu, Y. He and X. Fu, *J. Phys. Chem. C*, 2010, **114**, 2154-2159.
36. J. Yang, C. Chen, H. Ji, W. Ma and J. Zhao, *J. Phys. Chem. B*, 2005, **109**, 21900-21907.
37. J. C. Barreto, G. S. Smith, N. H. P. Strobel, P. A. McQuillin and T. A. Miller, *Life Sci.*, 1994, **56**, PL89-PL96.